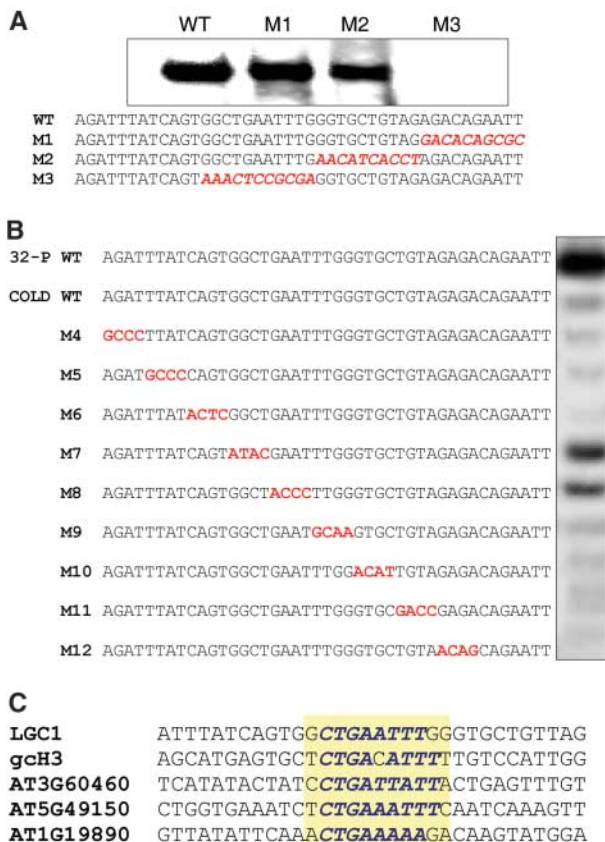


that represses transcription from promoters of numerous neuron-specific genes in neural precursors and non-neuronal cells (19) (fig. S7). Silencing of neural-specific genes is mediated via recruitment

of the corepressor CoREST, which functions as a molecular beacon for the recruitment of specialized silencing machinery (19). The question of whether GRSF-induced silencing of male germline-specific

genes in the rest of the plant cells involves associated corepressor(s) and the nature of the silencing machinery required for long-term repression remain exciting areas for further investigation.

**Fig. 4.** Identification of core binding domain of GRSF within the silencer region of *LGC1* promoter and conservation of core silencer domain in male germline genes. **(A)** EMSA using recombinant GRSF shows specific binding to 43-bp oligonucleotide sequence of the *LGC1* promoter (WT). Mutations in the region GGCTGAATT of the oligonucleotide abolished specific binding (M3); mutations in other regions (M1 and M2) had no effect on binding. Mutated sequences are in red. **(B)** *LGC1* oligonucleotides (43 bp) carrying 4-bp mutation blocks (marked in red) used as cold competitors in EMSAs with concentration ratios of 100:1. Mutated oligonucleotides 7 and 8 exhibited the lowest capacity to compete with labeled WT probe. An 8-bp sequence covered by these two oligonucleotides lies within the 10-bp region GGCTGAATT identified by 10-bp block mutations. **(C)** Conservation of GRSF minimal binding site in the promoter regions of lily and *Arabidopsis* male germline-specific genes. *AT1G19890* encodes *Arabidopsis* male germline-specific H3 histone, *AT5G49150* encodes *Arabidopsis* male germline-specific unknown gene, and *AT3G60460* encodes *Arabidopsis* *DUO1* gene expressed in male germline cells. Core binding domain is shaded in yellow, with conserved sequences marked in blue italics.



#### References and Notes

1. J. P. Mascarenhas, *Plant Cell* **1**, 657 (1989).
2. T. Mori, H. Kuroiwa, T. Higashiyama, T. Kuroiwa, *Nat. Cell Biol.* **8**, 64 (2006).
3. H. Xu, I. Swoboda, P. L. Bhalla, M. B. Singh, *Proc. Natl. Acad. Sci. U.S.A.* **96**, 2554 (1999).
4. H. Xu, I. Swoboda, P. L. Bhalla, M. B. Singh, *Plant Mol. Biol.* **39**, 607 (1999).
5. N. Rotman *et al.*, *Curr. Biol.* **15**, 244 (2005).
6. M. L. Engel, R. Holmes-Davis, S. McCormick, *Plant Physiol.* **138**, 2124 (2005).
7. M. Singh, P. L. Bhalla, H. Xu, M. B. Singh, *FEBS Lett.* **542**, 47 (2003).
8. W. Cook, J. Walker, *Nucleic Acids Res.* **20**, 359 (1992).
9. Y. V. Shidlovskii *et al.*, *EMBO J.* **24**, 97 (2005).
10. B. Boyle, N. Brisson, *Plant Cell* **13**, 2525 (2001).
11. C. Sun *et al.*, *J. Biol. Chem.* **276**, 24059 (2001).
12. A. Siddiqi *et al.*, *Nature* **410**, 383 (2001).
13. C. D. Strader, T. M. Fong, M. R. Tota, D. Underwood, R. A. F. Dixon, *Annu. Rev. Biochem.* **63**, 101 (1994).
14. M. Buttinielli, G. Panetta, D. Rhodes, A. Travers, *Genetica* **106**, 117 (1999).
15. P. Burkhard *et al.*, *Trends Cell Biol.* **11**, 82 (2001).
16. N. Imin, T. Kerim, J. J. Weinmann, B. G. Rolfe, *Mol. Cell. Proteomics* **5**, 274 (2006).
17. T. Okada, P. L. Bhalla, M. B. Singh, *Plant Cell Physiol.* **46**, 797 (2005).
18. T. Okada, M. Endo, M. B. Singh, P. L. Bhalla, *Plant J.* **44**, 557 (2005).
19. V. V. Lunnyak, M. G. Rosenfeld, *Cell* **121**, 499 (2005).
20. We thank S. Russell and B. Rolfe for critical reading of the manuscript and suggestions. Supported by the Australian Research Council.

#### Supporting Online Material

www.sciencemag.org/cgi/content/full/313/5786/496/DC1  
Materials and Methods  
Figs. S1 to S7  
References

30 January 2006; accepted 30 May 2006  
10.1126/science.1125526

## REPORTS

# Violation of Kirchhoff's Laws for a Coherent *RC* Circuit

J. Gabelli,<sup>1</sup> G. Fève,<sup>1</sup> J.-M. Berroir,<sup>1</sup> B. Plaçais,<sup>1</sup> A. Cavanna,<sup>2</sup>  
B. Etienne,<sup>2</sup> Y. Jin,<sup>2</sup> D. C. Glattli<sup>1,3\*</sup>

What is the complex impedance of a fully coherent quantum resistance-capacitance (*RC*) circuit at gigahertz frequencies in which a resistor and a capacitor are connected in series? While Kirchhoff's laws predict addition of capacitor and resistor impedances, we report on observation of a different behavior. The resistance, here associated with charge relaxation, differs from the usual transport resistance given by the Landauer formula. In particular, for a single-mode conductor, the charge-relaxation resistance is half the resistance quantum, regardless of the transmission of the mode. The new mesoscopic effect reported here is relevant for the dynamical regime of all quantum devices.

For a classical circuit, Kirchhoff's laws prescribe the addition of resistances in series. Its failure has been a central issue in developing our understanding of electronic

transport in mesoscopic conductors. Indeed, coherent multiple electronic reflections between scatterers in the conductor were found to make the conductance nonlocal (1, 2). A new compo-

sition law of individual scatterer contribution to resistance was found that led to the solution of the problem of electron localization (3) and, later, to formulation of the electronic conduction in terms of scattering of electronic waves (4). Nonadditivity of series resistances, or of parallel conductances, nonlocal effects, and negative four-point resistances (5) have been observed in a series of transport experiments at low temperature, where phase coherence extends over the mesoscopic scale (6, 7). It is generally accepted that the conductance of a phase-coherent quantum conductor is given by the Landauer formula and its generalization to multilead conductors (8), which relate the conductance to the transmission of electronic waves by the conductance quantum  $e^2/h$ . But, how far is this description robust at finite frequency, where conductance combines with nondissipative circuit elements such as capacitors or inductors? Are there significant

departures from the dc result? The question is important, as recent advances in quantum information highlight the need for fast manipulation of quantum systems, in particular quantum conductors. High-frequency quantum transport has been theoretically addressed, showing that a quantum RC circuit displays discrepancies with its classical counterpart (9, 10). It was shown that a counterintuitive modification of the series resistance led to the situation in which the resistance is no longer described by the Landauer formula and does not depend on transmission in a direct way (9, 10). Instead, it is directly related to the dwell time of electrons in the capacitor. Moreover, when the resistor transmits in a single electronic mode, a constant resistance was found, equal to the

<sup>1</sup>Laboratoire Pierre Aigrain, Département de Physique de l'École Normale Supérieure, 24 rue Lhomond, 75231 Paris Cedex 05, France. <sup>2</sup>Laboratoire de Photonique et Nanostructures, UPRESA CNRS, Route de Nozay, 91460 Marcoussis Cedex, France. <sup>3</sup>Service de Physique de l'Etat Condensé (CNRS URA 2464), Commissariat à l'Energie Atomique (CEA) Saclay, F91191 Gif-sur-Yvette, France.

\*To whom correspondence should be addressed. E-mail: glattli@lpa.ens.fr

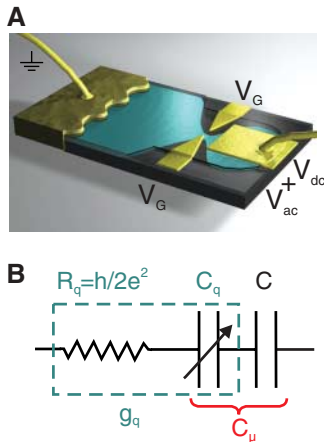


**Fig. 1.** The quantum capacitor realized using a 2DEG (A) and its equivalent circuit (B). The capacitor consists of a metallic electrode (in gold) on top of a submicrometer 2DEG quantum dot (in blue) defining the second electrode. The resistor is a QPC linking the dot to a wide 2DEG reservoir (in blue), itself connected to a metallic contact (dark gold). The QPC voltage  $V_G$  controls the number of electronic modes and their transmission. The radio frequency voltage  $V_{ac}$  and eventually a dc voltage  $V_{dc}$  are applied to the counter-electrode, whereas the ac current, from which the complex conductance is deduced, is collected at the ohmic contact. As predicted by the theory, the relaxation resistance  $R_q$ , which enters the equivalent circuit for the coherent conductance, is transmission-independent and equal to half the resistance quantum. The capacitance is the serial combination  $C_\mu$  of the quantum and the geometrical capacitances ( $C_q$  and  $C$ , respectively).  $C_q$  is transmission-dependent and strongly modulated by  $V_{dc}$  and/or  $V_G$ . The combination of  $R_q$  and  $C_q$  forms the impedance  $1/g_q$  of the coherent quantum conductor.

half-resistance quantum  $h/2e^2$ , i.e., it was not transmission-dependent. This resistance, modified by the presence of the coherent capacitor, was termed a “charge-relaxation resistance” to distinguish it from the usual dc resistance, which is sandwiched between macroscopic reservoirs and described by the Landauer formula. The quantum charge-relaxation resistance, as well as its generalization in nonequilibrium systems, is an important concept that can be applied to quantum information. For example, it enters into the problem of quantum-limited detection of charge qubits (11, 12), in the study of high-frequency-charge quantum noise (13–15), or in the study of dephasing of an electronic quantum interferometer (16). In molecular electronics, the charge-relaxation resistance is also relevant to the THz frequency response of systems such as carbon nanotubes (17).

We report on the observation and quantitative measurement of the quantum charge-relaxation resistance in a coherent RC circuit realized in a two-dimensional electron gas (2DEG) (see Fig. 1A). The capacitor is made of a macroscopic metallic electrode on top of a 2DEG submicrometer dot defining the second electrode. The resistor is a quantum point contact (QPC) connecting the dot to a wide 2DEG macroscopic reservoir. We address the coherent regime in which electrons emitted from the reservoir to the dot are backscattered without loss of coherence. In this regime, we have checked the prediction made in refs. (9, 10) that the charge-relaxation resistance is not given by the Landauer formula resistance but instead is constant and equals  $h/2e^2$ , as the QPC transmission is varied. Note that we consider here a spin-polarized regime and that the factor 1/2 is not the effect of spin, but a hallmark of a charge-relaxation resistance. When coherence is washed out by thermal broadening, the more conventional regime pertaining to dc transport is recovered. The present work differs from previous capacitance measurements where, for spectroscopic purpose, the dot reservoir coupling was weak and the ac transport regime was incoherent (18, 19). As a consequence, although quantum effects in the

capacitance were observable, the quantum charge-relaxation resistance was not accessible in these earlier experiments.

At zero temperature in the coherent regime and when a single mode is transmitted by the QPC, the mesoscopic RC circuit is represented by the equivalent circuit of Fig. 1B (9, 10). The geometrical capacitance  $C$  is in series with the quantum admittance  $g_q(\omega)$  connecting the ac current flowing in the QPC to the ac internal potential of the dot:

$$g_q(\omega) = 1 / \left( \frac{h}{2e^2} + \frac{1}{-i\omega C_q} \right), (T = 0) \quad (1)$$

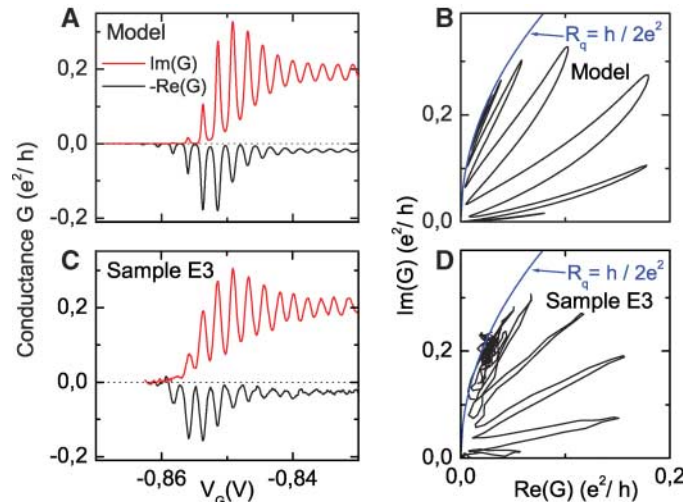
The nonlocal quantum impedance behaves as if it were the series addition of a quantum capacitance  $C_q$  with a constant contact resistance  $h/2e^2$ .  $C_q = e^2(dN/d\epsilon)$  is associated with the local density of state  $dN/d\epsilon$  of the mode propagating in the dot, taken at the Fermi energy. The striking effect of phase coherence is that the QPC transmission probability  $D$  affects the quantum capacitance (see Eq. 4) but not the resistance. The total circuit admittance  $G$  is simply:

$$G = \frac{-i\omega C g_q(\omega)}{-i\omega C + g_q(\omega)} = \frac{-i\omega C_\mu (2e^2/h)}{-i\omega C_\mu + (2e^2/h)}, (T = 0) \quad (2)$$

where  $C_\mu = CC_q/(C + C_q)$  is the electrochemical capacitance. In the incoherent regime, both resistance and quantum capacitance vary with transmission. The dot forms a second reservoir and the electrochemical capacitance  $C_\mu$  is in series with the QPC resistance  $R$ . In particular, when the temperature is high enough to smooth the capacitor density of states, the Landauer formula  $R = h/e^2 \times 1/D$  is recovered.

Several samples have been measured at low temperatures, down to 30 mK, which show analogous features. We present results on two samples made with 2DEG defined in the same high-mobility GaAsAl/GaAs heterojunction, with nominal density  $n_s = 1.7 \times 10^{15} \text{ m}^{-2}$  and mobility  $\mu = 260 \text{ V}^{-1} \text{ m}^2 \text{ s}^{-1}$ . A finite magnetic field ( $B = 1.3 \text{ T}$ )

**Fig. 2.** Complex conductance of sample E3 as function of the gate voltage  $V_G$  for  $T = 100 \text{ mK}$  and  $\omega/2\pi = 1.2 \text{ GHz}$ , at the opening of the first conduction channel (C) and its Nyquist representation in (D). The theoretical circle characteristic of the coherent regime is shown as a solid line. (A and B) show the corresponding curves for the simulation of sample E3 using the 1D model with  $C = 4fF$ ,  $C_\mu = 1fF$ .



is applied, so as to work in the ballistic quantum Hall regime with no spin degeneracy (20).

The real and imaginary parts of the admittance  $Im(G)$  and  $Re(G)$  as a function of QPC gate voltage  $V_G$  at the opening of the first conduction channel are shown in Fig. 2C. On increasing  $V_G$ , we can distinguish three regimes. At very negative  $V_G \leq -0.86$  V, the admittance is zero. Starting from this pinched state, peaks are observed in both  $Im(G)$  and  $Re(G)$ . Following a maximum in the oscillations, a third regime occurs where  $Im(G)$  oscillates nearly symmetrically about a plateau, whereas the oscillation amplitude decreases smoothly. Simultaneously, peaks in  $Re(G)$  quickly disappear to vanish in the noise.

Comparing these observations with the results of refs. (9,10), using a simplified one-dimensional (1D) model for  $C_q$  with one conduction mode and a constant energy level spacing in the dot  $\Delta$  (21), the simulation (Fig. 2A) shows a striking similarity to the experimental conductance traces in Fig. 2C. In this simulation,  $V_G$  determines the transmission  $D$  but also controls linearly the 1D dot potential. The transmission is chosen to vary with  $V_G$  according to a Fermi-Dirac-like dependence appropriate to describe QPC transmission (22). This model can be used to get a better under-

standing of the different conductance regimes. Denoting  $r$  and  $t$  the amplitude reflection and transmission coefficients of the QPC ( $r^2 = 1 - D$ ,  $t = \sqrt{D}$ ), we first calculate the scattering amplitude of the RC circuit:

$$s(\varepsilon) = r - t^2 e^{i\varphi} \sum_{n=0}^{\infty} (re^{i\varphi})^n = \frac{r - e^{i\varphi}}{1 - re^{i\varphi}} \quad (3)$$

where  $\varepsilon$  is the Fermi energy relative to the dot potential and  $\varphi = 2\pi\varepsilon/\Delta$  is the phase accumulated for a single turn in the quantum dot. The zero-temperature quantum capacitance is then given by:

$$C_q = e^2 (dN/d\varepsilon) = \frac{1}{2i\pi} s^+ \frac{\partial s}{\partial \varepsilon} = \frac{e^2}{\Delta} \times \frac{1 - r^2}{1 - 2r \cos(2\pi\varepsilon/\Delta) + r^2} \quad (4)$$

Therefore,  $C_q$  exhibits oscillations when the dot potential is varied. When  $r \rightarrow 0$ , these oscillations vanish and  $C_q \rightarrow e^2/\Delta$ . As reflection increases, oscillations are growing with maxima  $(e^2/\Delta)[(1+r)/(1-r)]$  and minima  $(e^2/\Delta)[(1-r)/(1+r)]$ . For strong reflection, Eq. 4 gives resonant Lorentzian peaks with an energy width  $D\Delta/2$  given by the escape rate of

$$g_q(\omega) = \int d\varepsilon \left( -\frac{\partial f}{\partial \varepsilon} \right) \times \frac{1}{h/2e^2 + 1/(-i\omega C_q)}, \quad (T \neq 0) \quad (5)$$

where  $f$  is the Fermi-Dirac distribution. Again the nonlocal admittance behaves as if it were the serial association of a charge-relaxation resistance  $R_q$  and a capacitance that we still denote  $C_q$ . In the weak transmission regime ( $D \rightarrow 0$ ), when  $D\Delta \ll k_B T$ , Eq. 5 yields thermally broadened capacitance peaks with

$$C_q \approx \frac{e^2}{4k_B T \cosh^2(\delta\varepsilon/2k_B T)}, \quad (D \ll 1) \quad (6)$$

where  $\delta\varepsilon$  denotes the energy distance to a resonant dot level. Note that these capacitance peaks do not depend on the dot parameters and can be used as a primary thermometer. Similar but transmission-dependent peaks are predicted in the inverse resistance

$$1/R_q \approx D \frac{e^2}{h} \times \frac{\Delta}{4k_B T \cosh^2(\delta\varepsilon/2k_B T)}, \quad (D \ll 1) \quad (7)$$

**Fig. 3.** Coulomb-blockade oscillations in the real part of the ac conductance in the low-transmission regime. The control voltage is applied to the counter-electrode for sample E3 (A) and to the QPC gate for sample E1 (B). The temperature dependence is used for absolute calibration of our setup, as described in the text: The peak width, shown in (C and D) as a function of temperature, is deduced from theoretical fits (solid lines) using Eq. 7 and taking a linear dependence of energy with the control voltage. Lines in (C) and (D) are fits of the experimental results using a  $\sqrt{(T^2 + T_0^2)}$  law to take into account a finite residual electronic temperature  $T_0$ .

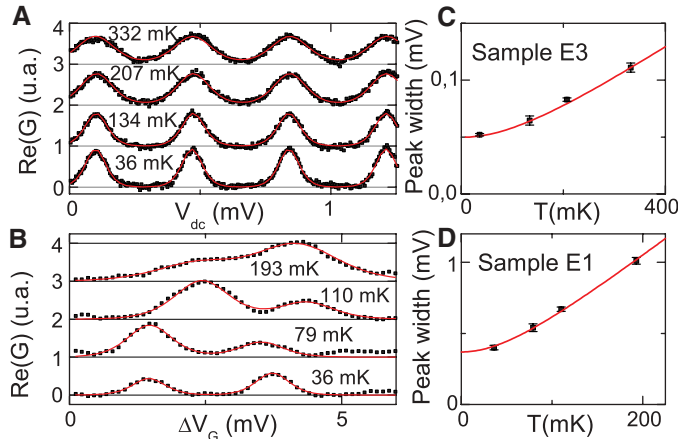
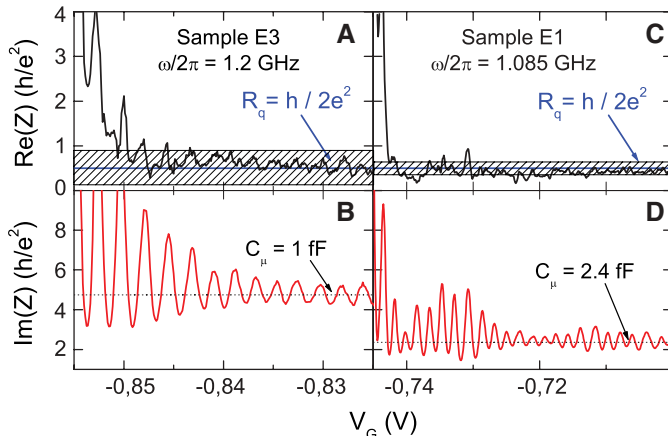


**Fig. 4.** Complex impedance of sample E3 (A and B) and sample E1 (C and D) as a function of QPC voltage for  $T = 30$  mK and  $B = 1.3$  T. The dashed lines in (B and D) correspond to the values of  $C_\mu$  deduced from calibration. The horizontal solid lines in (A and C) indicate the half-quantum of resistance expected for the coherent regime. Uncertainties on  $R_q$  are displayed as hatched areas.



conditions, the simulated traces are virtually free of adjustable parameters as  $C \geq 4C_\mu \gg C_q$ .

It is important to note that in a real system, the weak transmission regime is accompanied by Coulomb blockade effects that are not taken into account in the above model. In the weak transmission regime and  $T = 0$ , using an elastic cotunneling approach (23, 24), we have checked that there is no qualitative change except for the energy scale that now includes the charging energy so that  $\Delta$  is replaced by  $\Delta + e^2/C = e^2/C_\mu$ . At large transmission, the problem is nonperturbative in tunnel coupling and highly nontrivial. Calculations of the thermodynamic capacitance exist [(25, 26), and (27) plus references therein], but at present, no comprehensive model is available that would include both charge-relaxation resistance and quantum capacitance for finite temperature and/or large transmission.

Calibration of our admittance measurements is a crucial step toward extracting the absolute value of the constant charge-relaxation resistance. As at GHz frequencies, direct calibration of the whole detection chain is hardly better than 3 dB, we shall use here an indirect, but absolute, method, often used in Coulomb blockade spectroscopy, that relies on the comparison between the gate voltage width of a thermally broadened Coulomb peak ( $\propto k_B T$ ) and the Coulomb peak spacing ( $\propto e^2/C_\mu$ ). From this, an absolute value of  $C_\mu$  can be obtained. The real part of the admittance of sample E3 is shown as a function of the dc voltage  $V_{dc}$  at the counter-electrode, for a given low transmission (Fig. 3A). A series of peaks with periodicity  $\Delta V_{dc} = 370 \mu\text{V}$  are observed, with the peaks accurately fitted by Eq. 7. Their width, proportional to the electronic temperature  $T_{\text{el}}$ , is plotted versus the refrigerator temperature  $T$  (see Fig. 3C). When corrected for apparent electron heating arising from gaussian environmental charge noise, and if we assume  $T_{\text{el}} = \sqrt{(T^2 +$

$T_0^2)$ , the energy calibration of the gate voltage yields  $C_\mu$  and the amplitude  $1/C_\mu \omega$  of the conductance plateau in Fig. 2. A similar analysis is done in Fig. 3, B and D, for sample E1 using  $V_G$  to control the dot potential. Here, peaks are distorted because of a transmission-dependent background and show a larger periodicity  $\Delta V_G = 2 \text{ mV}$ , which reflects the weaker electrostatic coupling to the 2DEG.

Finally, after numerical inversion of the conductance data, we can separate the complex impedance into the contributions of the capacitance,  $1/C_\mu \omega$ , and the relaxation resistance  $R_q$ . The results in Fig. 4 demonstrate deviations from standard Kirschhoff's laws: The charge-relaxation resistance  $R_q$  remains constant in the regime where the quantum capacitance exhibits strong transmission-dependent oscillations; this constant value equals, within experimental uncertainty, half the resistance quantum as prescribed by theory (9, 10). In the weak transmission regime, the Landauer formula is recovered because of thermal broadening, and  $R_q$  diverges as it does in the dc regime. Furthermore, additional measurements at 4 K prove that the classical behavior is indeed recovered in the whole transmission range whenever  $k_B T \gg e^2/C_\mu$ .

In conclusion, we have experimentally shown that the series association of a quantum capacitor and a model quantum resistor leads to a violation of the dynamical Kirchhoff's law of impedance addition. In the fully coherent regime, the quantum resistor is no longer given by the Landauer formula but by the half-quantized charge-relaxation resistance predicted in refs. (9, 10).

#### References and Notes

1. R. Landauer, *IBM J. Res. Dev.* **1**, 233 (1957).
2. R. Landauer, *Phil. Mag.* **21**, 863 (1970).
3. P. W. Anderson, *Phys. Rev. B* **23**, 4828 (1981).
4. M. Büttiker, Y. Imry, R. Landauer, S. Pinhas, *Phys. Rev. B* **31**, 6207 (1985).

5. B. Gao, A. Kornik, R. Egger, D. C. Glatli, A. Bachtold, *Phys. Rev. Lett.* **92**, 216804 (2004).
6. See for a review, S. Datta, *Electronic Transport in Mesoscopic Systems* (Cambridge Univ. Press, Cambridge, 1997).
7. See for a review, Y. Imry, *Introduction to Mesoscopic Physics* (Oxford Univ. Press, Oxford, 1997).
8. M. Büttiker, *Phys. Rev. Lett.* **57**, 1761 (1986).
9. M. Büttiker, A. Prêtre, H. Thomas, *Phys. Rev. Lett.* **70**, 4114 (1993).
10. A. Prêtre, H. Thomas, M. Büttiker, *Phys. Rev. B* **54**, 8130 (1996).
11. S. Pilgram, M. Büttiker, *Phys. Rev. Lett.* **89**, 200401 (2002).
12. A. A. Clerk, S. M. Girvin, A. D. Stone, *Phys. Rev. B* **67**, 165324 (2003).
13. M. Büttiker, H. Thomas, A. Prêtre, *Phys. Lett. A* **180**, 364 (1993).
14. Ya. M. Blanter, M. Büttiker, *Phys. Rep.* **336**, 1 (2000).
15. F. W. J. Hekking, J. P. Pekola, *Phys. Rev. Lett.* **96**, 056603 (2006).
16. G. Seelig, S. Pilgram, A. N. Jordan, M. Büttiker, *Phys. Rev. B* **68**, 161310 (2003).
17. P. J. Burke, *IEEE T. Nanotechnol.* **2** (1), 55 (2003).
18. R. C. Ashoori et al., *Phys. Rev. Lett.* **68**, 3088 (1992).
19. R. C. Ashoori et al., *Phys. Rev. Lett.* **71**, 613 (1992).
20. Materials and methods are available as supporting material on Science Online.
21. J. Gabelli, thesis, Université Pierre et Marie Curie, Paris, 2006; online access at (<http://tel.ccsd.cnrs.fr/tel/00011619>).
22. M. Büttiker, *Phys. Rev. B* **41**, 7906 (1990).
23. D. V. Averin, Y. Nazarov, in *Single Charge Tunneling* (NATO ASI ser. B, vol. 294, Plenum, New York, 1992), chap. 6.
24. D. C. Glatli, *Physica B* **189**, 88 (1993).
25. K. A. Matveev, *Phys. Rev. B* **51**, 1743 (1995).
26. L. I. Glazman, I. L. Aleiner, *Phys. Rev. B* **57**, 9608 (1998).
27. P. W. Brouwer, A. Lamacraft, K. Flensberg, *Phys. Rev. B* **72**, 075316 (2005).
28. The Laboratoire Pierre Aigrain is the CNRS-ENS UMR8551 associated with universities Paris 6 and Paris 7. The research has been supported by AC-Nanoscience, SESAME grants, and ANR-05-NANO-028.

#### Supporting Online Material

[www.sciencemag.org/cgi/content/full/1126940/DC1](http://www.sciencemag.org/cgi/content/full/1126940/DC1)  
Materials and Methods

2 March 2006; accepted 26 June 2006

Published online 13 July 2006;

10.1126/science.1126940

Include this information when citing this paper.

## Second-Harmonic Generation from Magnetic Metamaterials

Matthias W. Klein,<sup>1,2</sup> Christian Enkrich,<sup>1,2</sup> Martin Wegener,<sup>1,2,3</sup> Stefan Linden<sup>1,2,3\*</sup>

We observe second-harmonic generation from metamaterials composed of split-ring resonators excited at 1.5-micrometer wavelength. Much larger signals are detected when magnetic-dipole resonances are excited, as compared with purely electric-dipole resonances. The experiments are consistent with calculations based on the magnetic component of the Lorentz force exerted on metal electrons—an intrinsic second-harmonic generation mechanism that plays no role in natural materials. This unusual mechanism becomes relevant in our work as a result of the enhancement and the orientation of the local magnetic fields associated with the magnetic-dipole resonances of the split-ring resonators.

The concept of metamaterials has changed the spirit of optics and photonics. Researchers no longer just study the rich variety of materials provided by nature but have rather become creative designers who tailor optical properties at will, leading to qualitatively new and

unprecedented behavior (1–11). The key is the nanofabrication of metallic subwavelength-scale functional building blocks, photonic atoms, which are densely packed into an effective material. To a large extent, this emerging field has been stimulated by the 1999 theoretical work of John

Pendry's group (1), which made two distinct predictions: (i) They proposed split-ring resonators as photonic atoms that could lead to magnetism at optical frequencies—a prerequisite for negative-index metamaterials. (ii) Furthermore, they predicted that enhanced and novel nonlinear-optical properties could arise from such metamaterials. Although aspect (i) has attracted substantial attention from both experiment (3–7, 12, 13) and theory (14–16) in recent years, aspect (ii) has not, to the best of our knowledge. Experiments have not been reported, nor has a complete consistent microscopic theory of the nonlinear optics of metamaterials been evaluated. This lack of re-

<sup>1</sup>Institut für Angewandte Physik, Universität Karlsruhe (TH), Wolfgang-Gaede-Straße 1, D-76131 Karlsruhe, Germany.

<sup>2</sup>DFG-Center for Functional Nanostructures (CFN), Universität Karlsruhe (TH), D-76128 Karlsruhe, Germany. <sup>3</sup>Institut für Nanotechnologie, Forschungszentrum Karlsruhe, in der Helmholtz-Gemeinschaft, D-76021 Karlsruhe, Germany.

\*To whom correspondence should be addressed. E-mail: stefan.linden@physik.uni-karlsruhe.de